Structure−Reactivity Studies in Copper(II)-Catalyzed Phosphodiester Hydrolysis

Eric L. Hegg, Stephen H. Mortimore, Chin Li Cheung, Jennifer E. Huyett, Douglas R. Powell, and Judith N. Burstyn*

Department of Chemistry, University of Wisconsin−Madison, 1101 University Avenue, Madison, Wisconsin 53706

Received September 9, 1998

We have investigated the ability of a series of three related copper complexes Cu([9−11]aneN$_3$)X$_2$ to hydrolyze the activated phosphodiesters bis(4-nitrophenyl) phosphate (BNPP) and ethyl 4-nitrophenyl phosphate (ENPP). The compound Cu([10]aneN$_3$)Br$_2$ crystallizes in the monoclinic space group *C*2/*c*, $a = 20.693(4)$ Å, $b = 11.429(2)$ Å, $c = 20.138(4)$ Å, $\beta = 104.78(3)°$, $V = 4605(2)$ Å^3, and $Z = 16$. The compound Cu([11]aneN$_3$)Br$_2$ crystallizes in the orthorhombic space group *Pnma*, $a = 13.7621(10)$ Å, $b = 8.7492(13)$ Å, $c = 10.0073(10)$ Å, $V = 1205.0(2)$ Å^3, and $Z = 4$. The structure of Cu([9]aneN$_3$)Cl$_2$ was previously reported (*Inorg. Chem.* **1980**, *19*, 1379). The crystal structures of the three complexes show a progression in geometry from square pyramidal to distorted trigonal bipyramidal as the size of the macrocycle increases. Larger macrocycles also result in the copper ion being pulled closer to the plane defined by the three ligand nitrogens, which in turn results in an increase in the sum of the three N−Cu−N angles from 249° to 257° to 278° along with a concomitant decrease in the X−Cu−X angle. Significantly, the rate constant for the hydrolysis of BNPP by Cu([9−11]aneN$_3$)X$_2$ increases by nearly an order of magnitude as the ligand size increases from a nine-membered to an 11-membered ring. Correlations have been made between the catalytic ability of Cu([9−11]aneN$_3$)X$_2$ and the structural and electronic properties of the complexes. All three catalysts exist in a monomer−dimer equilibrium in solution, with the monomer being the catalytically active species. As the ligand size increases, the dimer formation constant (K_f) decreases due to steric constraint, thereby increasing the concentration of active species and hence the rate of hydrolysis. The contributions of Lewis acidity and steric constraint on both substrate binding (K_2) and P−O bond cleavage (k_3 or k_{cat}) are less important than the dimerization equilibrium constant in determining the rate of the reaction.

Introduction

The half-life for the hydrolysis of dimethyl phosphate is estimated to be 130 000 years at neutral pH and 25 °C.[1] The impressive stability of the phosphodiester bond is a result of the negative charge on the phosphate group which repels potential nucleophiles.[2] Nucleases, however, are able to hydrolyze DNA with rate enhancements over the uncatalyzed reaction exceeding 10^{16} under physiological conditions.[3] Although many of these nucleases utilize one or more metal ions, the exact role these ions play is not clear.[4] It is the goal of those designing synthetic metallonucleases to uncover and exploit the mechanisms nature utilizes to effect such impressive rate enhancements.[5]

Recent efforts to design synthetic nucleases and elucidate the mechanisms by which metal ions promote hydrolysis have focused primarily on small metal complexes.[5−9] Hendry and Sargeson[10] studied intramolecular phosphodiester hydrolysis reactions using a substitutionally inert monoaquated phosphodiester−Ir(III) complex; it was demonstrated that the rate of hydrolysis is maximized when the pH of the reaction is above the pK_a of the coordinated H_2O, implicating a metal-bound hydroxide nucleophile. Studies with tetraamine−Co(III) complexes yielded similar results, showing a maximal rate in a pH range that is between the pK_a's of the first and second coordinated water molecules.[11,12] Together these results suggest a mechanism where, following substrate binding, hydrolysis occurs via intramolecular attack of a metal-coordinated hydroxide (Scheme 1). These experiments also provide the criteria for an effective synthetic nuclease; the metal complexes should have two open cis-oriented sites, one to bind the substrate and the other to bind water or hydroxide, and the complexes should be strong Lewis acids to provide electrophilic activation of the substrate as well as a coordinated hydroxide at near-neutral pH.[5]

The rate of phosphodiester hydrolysis also depends heavily on the polydentate ligand used to chelate the metal ion. The effect of ligand structure on phosphodiester hydrolysis was explored by Chin et al. using various tetraamine−Co(III) complexes,[11,12] and the rate of hydrolysis was found to increase with increasing N−Co−N angles.[12] The correlation between the N−Co−N angle and the rate of hydrolysis was attributed to the stability of the four-membered-ring transition state that is formed upon intramolecular attack by a metal-bound hydroxide

* Author to whom correspondence should be addressed. E-mail: Burstyn@chem.wisc.edu.

(1) Radzicka, A.; Wolfenden, R. *Science* **1995**, *267*, 90−93.
(2) Westheimer, F. H. *Science* **1987**, *235*, 1173−1178.
(3) Serpersu, E. H.; Shortle, D.; Mildvan, A. S. *Biochemistry* **1987**, *26*, 1289−1300.
(4) Tullius, T. D. In *Metals and Molecular Biology*; Tullius, T. D., Ed.; American Chemical Society: Washington, DC, 1989; pp 1−23.
(5) Hegg, E. L.; Burstyn, J. N. *Coord. Chem. Rev.* **1998**, *173*, 133−165.
(6) Hendry, P.; Sargeson, A. M. *Prog. Inorg. Chem.* **1990**, *38*, 201−258.
(7) Chin, J. *Acc. Chem. Res.* **1991**, *24*, 145−152.
(8) Kimura, E.; Koike, T. *Adv. Inorg. Chem.* **1997**, *44*, 229−261.
(9) Morrow, J. R. *Met. Ions Biol. Syst.* **1997**, *33*, 561−592.
(10) Hendry, P.; Sargeson, A. M. *J. Am. Chem. Soc.* **1989**, *111*, 2521−2527.
(11) Chin, J.; Zou, X. *J. Am. Chem. Soc.* **1988**, *110*, 223−225.
(12) Chin, J.; Banaszczyk, M.; Jubian, V.; Zou, X. *J. Am. Chem. Soc.* **1989**, *111*, 186−190.

10.1021/ic981087g CCC: $18.00
Published on Web 05/18/1999

Scheme 1. Generic Mechanism Inspired by Substitutionally Inert Metal Complexes

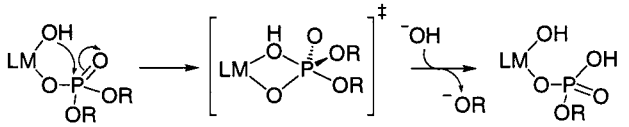

Scheme 2. Monomer−Dimer Equilibrium of $Cu([9]aneN_3)^{2+}$

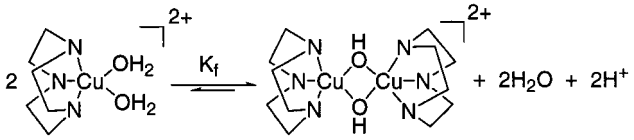

Scheme 3. Proposed Reaction Mechanism for the $Cu([9]aneN_3)^{2+}$-Catalyzed Hydrolysis of Activated Phosphodiesters

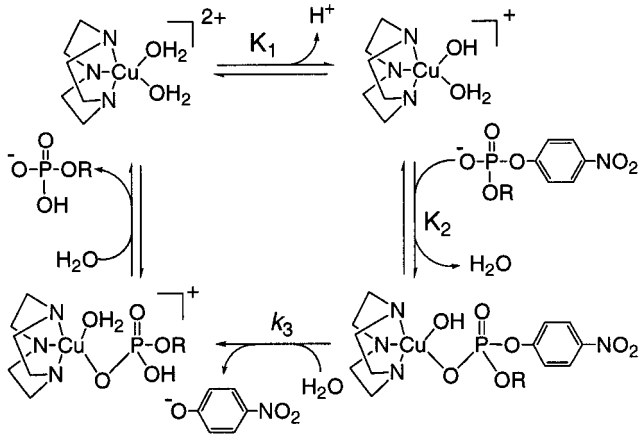

(Scheme 1). The bond angles of all four-membered rings must sum to no more than 360°, far less than the sum of the idealized geometries of the individual components in a strain-free system. Chin et al. hypothesized that a larger N−Co−N bond angle results in a decrease of the trans O−Co−O bond angle thus stabilizing the four-membered-ring intermediate.[12] Evidence for this hypothesis was afforded by measuring the stability of various Co(III)−carboxylate chelates;[13] as the N−Co−N angle increased, so did the stability of the chelate. In addition to the two criteria mentioned previously, the availability of two open cis-oriented sites and strong Lewis acidity, these studies provide a third criterion for effective phosphodiesterases, a ligand structure that accommodates formation of the four-membered phosphate ring intermediate.

We recently established that copper(II) 1,4,7-triazacyclononane dichloride ($Cu([9]aneN_3)Cl_2$) is an effective phosphodiesterase,[14−16] catalytically hydrolyzing the activated phosphodiester bis(4-nitrophenyl) phosphate (BNPP) with a calculated rate enhancement of 2000.[16] The mechanism of BNPP hydrolysis by $Cu([9]aneN_3)Cl_2$ has been studied in detail (Schemes 2 and 3).[16,17] The metal complex is in a monomer−dimer equilibrium with the monomer being the catalytically active species. Following substrate binding, the BNPP is hydrolyzed by an intramolecular attack of a metal-coordinated hydroxide. The reaction proceeds via a concerted mechanism where bond formation and bond cleavage occur simultaneously at the phosphorus center.[17] In addition to hydrolyzing BNPP, $Cu([9]aneN_3)Cl_2$ also hydrolyzes both RNA[14] and DNA,[15] and a deeper knowledge of the factors affecting the reactivity of $Cu([9]aneN_3)Cl_2$ is desirable.

To obtain a better understanding of phosphodiester hydrolysis by $Cu([9]aneN_3)Cl_2$, we systematically varied the physical properties of the catalyst and tested the ability of these modified complexes to hydrolyze BNPP. The goal was to determine how different properties of copper(II) macrocycles affect the rate of BNPP hydrolysis. The information gained from this and other studies investigating how structure affects reactivity in phosphodiester hydrolysis[11−13,18−23] can be used to develop more efficient catalysts and may provide insight into the differences in rates between synthetic and enzymatic nucleases. Herein we report kinetic studies on phosphodiester hydrolysis by three related copper(II) macrocycles: $Cu([9]aneN_3)Cl_2$, $Cu([10]aneN_3)Br_2$, and $Cu([11]aneN_3)Br_2$. Structural and electronic properties of these labile metal complexes are discussed, and the relationships between these properties and reactivity are also presented. In this study we specifically address the effects of structure at each step along the reaction pathway.

Experimental Section

Materials. The buffer CHES [2-(*N*-cyclohexylamino)ethanesulfonic acid] and the sodium salt of the phosphate diester BNPP were purchased from Sigma Chemical Co. All other chemicals were purchased from Aldrich and used without further purification. Water was purified by passage through a Millipore purification system.

Instrumentation. Mass spectroscopy of the metal complexes was performed with a VG AutoSpec spectrometer using electrospray ionization in a 50/50/0.2 H_2O/CH_3CN/formic acid matrix. A Nicolet 740 FT-IR spectrometer was used for infrared spectroscopy. Electron paramagnetic resonance (EPR) spectroscopy was performed on a Bruker EPR 300E spectrometer equipped with an EIP model 625A frequency counter. The magnetic field was calibrated with a Bruker NMR gaussmeter and the temperature maintained at 77 K with a liquid-nitrogen-filled dewar. For pH determinations, an Orion Research digital ion analyzer model 611 equipped with a Ross semimicro temperature compensation electrode was utilized. Kinetic measurements were made using a Hitachi U-3210 UV/visible spectrophotometer equipped with a water-jacketed cell holder. The temperature was regulated by an external circulating water bath (Lauda MT). Additional kinetic measurements were performed using Varian Cary 4 Bio and Varian Cary 5G UV/vis/near-IR spectrophotometers with 6 × 6 thermostated cell blocks for temperature control. Elemental analysis was performed by Galbraith Laboratories (Knoxville, TN).

Synthesis of $[9]aneN_3$, $[10]aneN_3$, and $[11]aneN_3$. The macrocyclic ligands $[9]aneN_3$, $[10]aneN_3$, and $[11]aneN_3$ were synthesized by the Richman−Adkins cyclization reaction using the appropriate ligand precursors.[24−26] For example, $[9]aneN_3$ was prepared by the cyclization

(13) Connolly, J. A.; Kim, J. H.; Banaszczyk, M.; Drouin, M.; Chin, J. *Inorg. Chem.* **1995**, *34*, 1094−1099.
(14) Hegg, E. L.; Deal, K. A.; Kiessling, L. L.; Burstyn, J. N. *Inorg. Chem.* **1997**, *36*, 1715−1718.
(15) Hegg, E. L.; Burstyn, J. N. *Inorg. Chem.* **1996**, *35*, 7474−7481.
(16) Deal, K. A.; Burstyn, J. N. *Inorg. Chem.* **1996**, *35*, 2792−2798.
(17) Deal, K. A.; Hengge, A. C.; Burstyn, J. N. *J. Am. Chem. Soc.* **1996**, *118*, 1713−1718.
(18) Young, M. J.; Wahnon, D.; Hynes, R. C.; Chin, J. *J. Am. Chem. Soc.* **1995**, *117*, 9441−9447.
(19) DeRosch, M. A.; Trogler, W. C. *Inorg. Chem.* **1990**, *29*, 2409−2416.
(20) Kesicki, E. A.; DeRosch, M. A.; Freeman, L. H.; Walton, C. L.; Harvey, D. F.; Trogler, W. C. *Inorg. Chem.* **1993**, *32*, 5851−5867.
(21) Hettich, R.; Schneider, H.-J. *J. Am. Chem. Soc.* **1997**, *119*, 5638−5647.
(22) Rammo, J.; Hettich, R.; Roigk, A.; Schneider, H.-J. *J. Chem. Soc., Chem. Commun.* **1996**, 105−107.
(23) Chapman, W. H., Jr.; Breslow, R. *J. Am. Chem. Soc.* **1995**, *117*, 5462−5469.
(24) Koyama, H.; Yoshino, T. *Bull. Chem. Soc. Jpn.* **1972**, *45*, 481−484.
(25) Searle, G. H.; Geue, R. J. *Aust. J. Chem.* **1984**, *37*, 959−970.
(26) Richman, J. E.; Adkins, T. J. *J. Am. Chem. Soc.* **1974**, *96*, 2268−2270.

of *N*,*N*′,*N*″-tris(*p*-toluenesulfonyl)diethylenetriamine and 1,2-bis(*p*-toluenesulfonyloxy)ethane while the synthesis of [10]aneN$_3$ utilized *N*,*N*′,*N*″-tris(*p*-toluenesulfonyl)diethylenetriamine and 1,3-bis(*p*-toluenesulfonyloxy)propane. Deprotection of the macrocycles was accomplished by refluxing in concentrated acid as previously described.[25,26] The [9]aneN$_3$ ligand was isolated as the trihydrochloride salt while [10]aneN$_3$ and [11]aneN$_3$ were isolated as the trihydrobromide salts.

Synthesis of Cu([9]aneN$_3$)Cl$_2$. The metal complex Cu([9]aneN$_3$)Cl$_2$ was prepared according to literature procedure.[16,27] In general, solid CuCl$_2$·2H$_2$O and 1 equiv of [9]aneN$_3$·3HCl were combined in an aqueous solution followed by the addition of 3 equiv of NaOH. The volume was reduced over a steam bath and NaCl selectively precipitated by the addition of ethanol. Blue X-ray quality crystals were obtained from an aqueous solution by slow evaporation of H$_2$O. Spectroscopic and crystallographic features were identical to those previously reported.[27]

Synthesis of Cu([10]aneN$_3$)Br$_2$. An aqueous solution of 0.17 M CuBr$_2$ (0.13 mmol) was added to an equimolar amount of [10]aneN$_3$·3HBr. The resulting solution was combined with 2.95 equiv of NaOH(aq) and stirred for at least 15 min. The blue solution was evaporated to dryness on a steam bath, resulting in a green precipitate. The precipitate was washed with methanol and dissolved in a minimum volume of water. The volume was doubled by the slow addition of ethanol, and the mixture was cooled to 4 °C. Green, prismatic, X-ray quality crystals were obtained after 120 h in 49% yield. UV/vis: $\lambda_{max(UV)}$ = 246 nm (ϵ = 3080); $\lambda_{max(vis)}$ = 665 nm (ϵ = 59.9). MS (ESI, H$_2$O/CH$_3$CN/formic acid, *m*/*z*): 251.1 (LCu^{2+} + HC(O)O$^-$). Anal. Calcd for C$_7$H$_{17}$N$_3$CuBr$_2$: C, 22.94; H, 4.67; N, 11.46; Cu, 17.33; Br, 43.59. Found: C, 22.95; H, 4.56; N, 11.56; Cu, 17.60; Br, 40.77.

Synthesis of Cu([11]aneN$_3$)Br$_2$. An aqueous solution of 0.14 M CuBr$_2$ (0.12 mmol) was added to an equimolar amount of [11]aneN$_3$·3HBr. The resulting solution was combined with 2.95 equiv of NaOH(aq) with stirring. The volume was reduced by $^1/_3$ on a steam bath and cooled to room temperature followed by the addition of ethanol to increase the volume approximately 1.5-fold. Cooling the solution at 4 °C gave green, prismatic, X-ray quality crystals. UV/vis: $\lambda_{max(UV)}$ = 247 nm (ϵ = 2710); $\lambda_{max(vis)}$ = 664 nm (ϵ = 85.6). MS (ESI, H$_2$O/CH$_3$CN/formic acid, *m*/*z*): 265.1 (LCu^{2+} + HC(O)O$^-$). Anal. Calcd for C$_8$H$_{19}$N$_3$CuBr$_2$: C, 25.25; H, 5.03; N, 11.04; Cu, 16.70; Br, 41.99. Found: C, 25.03; H, 5.04; N, 10.96; Cu, 16.90; Br, 42.55.

Synthesis of Sodium Ethyl 4-Nitrophenyl Phosphate (ENPP). ENPP was synthesized using the procedure described by Hendry and Sargeson[10] and purified via reverse phase liquid chromatography. Approximately 1.5 g of crude ENPP was dissolved in a minimum volume of H$_2$O, and the pH was adjusted to >7 with NaOH. This solution was loaded onto 250 g of reverse phase silica gel[28,29] and eluted with H$_2$O. The appropriate fractions (as determined by the A_{280} profile) were combined, concentrated via rotary evaporation, and lyophilized to give a white, powdery product (75% yield). ^{1}H NMR (300 MHz, D$_2$O): δ 1.08 (t, 3H), 3.87 (dq, 2H), 7.15 (d, 2H), 8.08 (d, 2H).

X-ray Crystallography. The crystal structures were solved by direct methods using the SHELXS-86 program.[30] They were refined by using the SHELXL-93 program[31] which refines on F^2 values. Neutral atom scattering factors were taken from the literature.[32] Values for R1(F) and wR2(F^2) are reported in Table 1; R1(F) is based on observed data [$I > 2\sigma(I)$], and wR2(F^2) is based on all data.

pH Titrations. Solutions of each copper complex were prepared at concentrations ranging from approximately 3 to 7 mM with the ionic strength adjusted to 0.1 M using NaClO$_4$. The solutions were titrated with both acid and base using 0.1 M HCl and 0.1 M NaOH, respectively, over the pH range 3−11. All titrations were performed in duplicate. A single pK_a value was determined for each titration curve. The pH meter was calibrated using commercial pH standards prior to each titration.

Table 1. Summary of Crystallographic Data for Cu([10−11]aneN$_3$)Br$_2$

	Cu([10]aneN$_3$)Br$_2$	Cu([11]aneN$_3$)Br$_2$
empirical formula	C$_7$H$_{17}$Br$_2$CuN$_3$	C$_8$H$_{19}$Br$_2$CuN$_3$
fw	366.60	380.60
temp (K)	113(2)	113(2)
cryst syst	monoclinic	orthorhombic
space group	*C*2/*c* (No. 15)	*Pnma* (No. 62)
unit cell dimens		
a (Å)	20.693(4)	13.7621(10)
b (Å)	11.429(2)	8.7492(13)
c (Å)	20.138(4)	10.0073(10)
α (deg)	90	90
β (deg)	104.78(3)	90
γ (deg)	90	90
vol (Å^3)	4605(2)	1205.0(2)
Z	16	4
wavelength (Å)	1.541 78	1.541 78
ρ(calc) (g/cm^3)	2.115	2.098
abs coeff (mm^{-1})	10.503	10.065
goodness of fit	1.163	1.068
R1 [$I > 2\sigma(I)$][a]	0.0786	0.0454
wR2 (all data)[b]	0.2076	0.1079

[a] $R1 = \sum||F_o| - |F_c||/\sum|F_o|$. [b] $wR2 = [[\sum w(F_o^2 - F_c^2)^2]/\sum[w(F_o^2)^2]]^{1/2}$.

EPR Spectroscopy. Solutions were prepared in both DMSO and H$_2$O/EtOH (50/50) at concentrations of approximately 0.5 mM. The frozen solution EPR measurements were taken at 77 K at X-band frequency. The spectra obtained were the average of 6−10 scans. The field values obtained were corrected with a gaussmeter calibrated against 1,1-diphenyl-2-picrylhydrazyl (DPPH), and the *g* values were calculated directly from the corrected field values and the measured frequency.

Kinetics of BNPP Hydrolysis. The initial rate of reaction between each metal complex and BNPP was monitored spectrophotometrically at 400 nm by the production of 4-nitrophenolate. The concentration of 4-nitrophenolate was calculated from the extinction coefficient (18 700 L mol^{-1} cm^{-1}) and was corrected for the degree of ionization at the reaction temperature and pH.[33] To correct for spontaneous hydrolysis of the phosphodiester, the rate of each reaction was measured against a reference cell which was identical in composition except lacking the metal complex. Reactions were performed in glass cells sealed with a Teflon lined screw cap. Each reaction was maintained at pH 9.2 with 50 mM CHES buffer and an ionic strength of 0.1 M with NaClO$_4$. Both the sample and reference cells were equilibrated at 50 °C before the addition of BNPP. After an additional 5 min of equilibration, the increase in absorbance at 400 nm was followed for no more than 1 h. Reactions were monitored to less than 5% conversion of substrate to product. All reactions were performed in triplicate, and the reported data represent the average of these trials.

The initial rate of reaction was obtained as the slope of a plot of 4-nitrophenolate concentration versus time, which was linear with R^2 > 0.999. Reaction order was determined with respect to both metal complex and BNPP, and the rate constants were determined from the initial rates. Kinetically determined dimer formation constants (K_f) were calculated from a linear least squares fit of plots of initial rate versus metal complex concentration to the one-half power. Only the linear regions of the graphs were utilized; at very low concentrations of metal complex the reactions become first order with respect to metal.

Substrate Saturation Kinetics Using ENPP. Saturation kinetics with the substrate ENPP were performed at pH 9.2 (buffered with 0.5 M CHES) and 50 °C with an ionic strength of 0.68 M (adjusted with 0.5 M NaClO$_4$). The ENPP concentration utilized was 4.5−150 mM, while the metal complex concentration was 0.5 mM for Cu([9]aneN$_3$)Cl$_2$ and Cu([11]aneN$_3$)Br$_2$ and 0.1 mM for Cu([10]aneN$_3$)Br$_2$. All

(27) Schwindinger, W. F.; Fawcett, T. G.; Lalancette, R. A.; Potenza, J. A.; Schugar, H. J. *Inorg. Chem.* **1980**, *19*, 1379−1381.
(28) Evans, M. B.; Dale, A. D.; Little, C. J. *Chromatographia* **1980**, *13*, 5−10.
(29) Kühler, T. C.; Lindsten, G. R. *J. Org. Chem.* **1983**, *48*, 3589−3591.
(30) Sheldrick, G. M. *Acta Crystallogr., Sect. A* **1990**, *46*, 467−473.
(31) Sheldrick, G. M. *SHELXL93. Program for the Refinement of Crystal Structures*; University of Göttingen: Göttingen, Germany, 1993.
(32) *International Tables for Crystallography*; Kluwer: Boston, 1992; Vol. C, Tables 6.1.1.4, 4.2.6.8, and 4.2.4.2.
(33) Martell, A. E.; Smith, R. M. *Critical Stability Constants*; Plenum Press: New York, 1977.

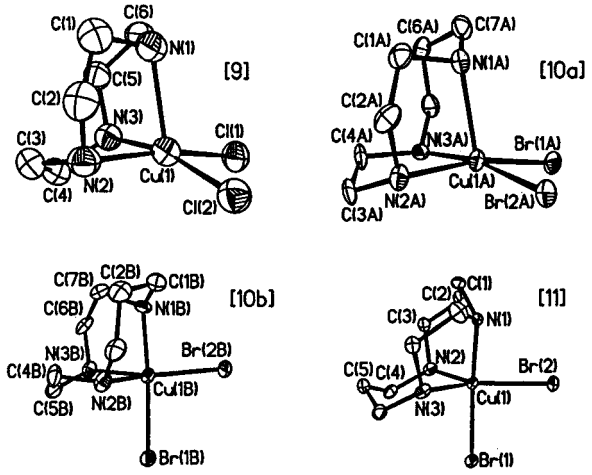

Figure 1. Crystal structures for Cu([9−11]aneN$_3$)X$_2$; [9] = Cu([9]-aneN$_3$)Cl$_2$, [10] = Cu([10]aneN$_3$)Br$_2$, and [11] = Cu([11]aneN$_3$)Br$_2$. All displacement ellipsoids were drawn at 50% probability. The structure for Cu([9]aneN$_3$)Cl$_2$ was taken from the literature;[27] the labels for atoms N2 and N3 have been reversed to allow a direct comparison with the structures reported herein. The unit cell of Cu([10]aneN$_3$)Br$_2$ contains two crystallographically independent molecules, [10a] and [10b]. [9] and [10a] are best described as distorted square pyramidal while [10b] and [11] are best described as distorted trigonal bipyramidal. In Cu([11]aneN$_3$)Br$_2$, atom N3 is related by symmetry to atom N2.

reactions were performed in duplicate as described above except that rates were not measured by direct difference due to the negligible rate of background hydrolysis. A nonlinear least squares fit of a plot of initial rate versus substrate concentration using the program HYPERL[34] gave values for K_m and V_{max} (data provided in Supporting Information). Because substrate binding perturbs the monomer−dimer equilibrium of the catalysts, which in turn affects the saturation curve, the calculated K_m and V_{max} values needed to be corrected. The appropriate correction factors were determined using a program to analytically solve the quadratic equation describing this set of complex equilibria and to generate simulated data (see Supporting Information). This simulated data was then fit using HYPERL. The differences between K_m and V_{max} calculated from HYPERL and the values defined in the program simulating the data gave the necessary correction factors. The catalytic rate constant, k_3 or k_{cat}, was obtained by dividing V_{max} by the total catalyst concentration.

Results

X-ray Crystallography. The crystal structures for Cu([9]-aneN$_3$)Cl$_2$, Cu([10]aneN$_3$)Br$_2$, and Cu([11]aneN$_3$)Br$_2$ (Figure 1) show an interesting progression in geometry from distorted square pyramidal toward distorted trigonal bipyramidal as the ligand ring size increases. A useful parameter to measure the extent of this progression is the τ-value,[35] which is essentially a measure of the difference between the two "basal" angles divided by 60. According to this criterion, a perfect square pyramid has a τ-value of 0.00 whereas a perfect trigonal bipyramid has a τ-value of 1.00. Thus, Cu([9]aneN$_3$)Cl$_2$ is a square pyramid (τ = 0.02) while Cu([11]aneN$_3$)Br$_2$, which sits on a crystallographic mirror plane, is best described as a distorted trigonal bipyramid (τ = 0.58). Interestingly, the unit cell of Cu([10]aneN$_3$)Br$_2$ contains two crystallographically independent molecules ([10a] and [10b]). One of the molecules, [10a], is square pyramidal (τ = 0.00) while the second, [10b], is best described as distorted trigonal bipyramidal (τ = 0.61).

A second important trend observed when comparing the structures of Cu([9]aneN$_3$)Cl$_2$, Cu([10]aneN$_3$)Br$_2$, and Cu([11]-aneN$_3$)Br$_2$ involves the position of the copper atom relative to the plane defined by the three ligand nitrogen atoms. As the ligand ring size increases and the rigidity of the macrocycle decreases, the copper atom moves closer to the plane of the nitrogen atoms; this trend can be observed by monitoring the increase in the sum of the three N−Cu−N bond angles from 249° to 257° to 278° as the macrocycle changes from a nine- to a 10- to an 11-membered ring. Significantly, with the increase in the N−Cu−N bond angles, there is also a corresponding decrease in the halogen−Cu−halogen bond angle from 94.23-(5)° for Cu([9]aneN$_3$)Cl$_2$ to 93.90(6)° and 93.51(6)° for Cu-([10]aneN$_3$)Br$_2$ (distorted trigonal bipyramidal and square pyramidal, respectively) to 90.50(5)° for Cu([11]aneN$_3$)Br$_2$. A summary of the crystallographic data and selected bond lengths and angles for the three metal complexes can be found in Tables 1 and 2.

Table 2. Selected Bond Lengths and Angles for Cu([9−11]aneN$_3$)X$_2$[a]

	[9][b]	[10a][c]	[10b][c]	[11][d]
		Bond Lengths		
Cu−N1	2.246(4)	2.216(8)	2.017(8)	2.057(8)
Cu−N2	2.063(4)	2.033(8)	2.116(8)	2.126(5)
Cu−N3	2.038(4)	2.053(8)	2.120(8)	2.126(5)
Cu−X1	2.268(1)	2.460(2)	2.455(2)	2.431(2)
Cu−X2	2.312(1)	2.449(2)	2.421(2)	2.491(2)
		Bond Angles		
N1−Cu−N2	83.0(2)	88.9(3)	88.7(3)	100.6(3)
N1−Cu−N3	82.6(2)	83.9(3)	83.9(3)	80.1(3)
N2−Cu−N3	82.2(2)	84.7(3)	84.4(3)	97.4(2)
X1−Cu−X2	94.23(5)	93.51(6)	93.90(6)	90.50(5)
N1−Cu−X1	105.8(1)	98.1(2)	175.8(2)	165.7(2)
N2−Cu−X1	90.5(1)	168.3(2)	89.2(2)	92.49(12)
N3−Cu−X1	168.2(1)	86.7(2)	92.4(2)	92.49(12)
N1−Cu−X2	107.2(1)	107.6(2)	90.0(2)	85.3(3)
N2−Cu−X2	167.0(1)	93.3(2)	139.4(2)	131.14(12)
N3−Cu−X2	91.0(1)	168.4(2)	135.8(2)	131.14(12)

[a] The nine-membered-ring complex is a dichloride salt, and the 10- and 11-membered rings are dibromide salts. [b] [9] = Cu([9]aneN$_3$)Cl$_2$. The bond lengths and angles for the structure of Cu([9]aneN$_3$)Cl$_2$ are the values previously reported;[27] our results are essentially identical. Atom labels N2 and N3 have been reversed to allow direct comparison with the structures reported here. [c] [10] = Cu([10]aneN$_3$)Br$_2$. Within the unit cell of Cu([10]aneN$_3$)Br$_2$, there are two crystallographically independent molecules, [10a] and [10b]. [d] [11] = Cu([11]aneN$_3$)Br$_2$. Cu([11]aneN$_3$)Br$_2$ sits on a crystallographic mirror plane. Atoms N1 and C2 are disordered (50/50) across this mirror plane. Atom N3 is related by symmetry to atom N2.

Spectroscopic Characterization. Despite the different geometries exhibited crystallographically within this series of metal complexes, in solution each is best characterized as a square pyramid. In their optical spectra, Cu([9−11]aneN$_3$)$^{2+}$ all exhibit a higher energy d−d transition accompanied by a lower energy and lower intensity shoulder (Table 3), characteristics indicative of Cu(II) square pyramidal complexes.[36] In contrast, Cu(II) trigonal bipyramidal complexes exhibit lower energy d−d peaks accompanied by higher energy shoulders while intermediate structures (i.e., significantly distorted with nonideal τ-values) tend to exhibit two equally intense transitions.[36] Interestingly, as the size of the macrocycle increases, all of the optical transitions shift to lower energy. This shift is a consequence of weakening σ-donor capability as the macrocycle increases in size,[37] thereby lowering the energies of the d−d transitions.

(34) Cleland, W. W. *Methods Enzymol.* **1979**, *63*, 103−138.
(35) Addison, A. W.; Rao, T. N.; Reedijk, J.; van Rijn, J.; Verschoor, G. C. *J. Chem. Soc., Dalton Trans.* **1984**, 1349−1356.
(36) Wei, N.; Murthy, N. N.; Karlin, K. D. *Inorg. Chem.* **1994**, *33*, 6093−6100.
(37) Zompa, L. J. *Inorg. Chem.* **1978**, *17*, 2531−2536.

Table 3. Summary of EPR and Absorption Spectra of the Various Metal Complexes

	EPR[a]			UV/vis[b]	
	$g_\perp$	$g_\parallel$	$A_\parallel$	λ_{max} (nm)	ϵ (M^{-1} cm^{-1})
$Cu([9]aneN_3)Cl_2$	2.062	2.249	160		
$Cu([9]aneN_3)(H_2O)_2$	2.062	2.293	149	254[c,d]	2650[c,d]
				654[c,e]	39.5[c,e]
				1074[e]	14.0[e]
$Cu([10]aneN_3)Br_2$	2.063	2.230	164		
$Cu([10]aneN_3)(H_2O)_2$	2.063	2.287	153	255[d]	3080[d]
				665[e]	59.9[e]
				1083[e]	24.3[e]
$Cu([11]aneN_3)Br_2$	2.063	2.230	160		
$Cu([11]aneN_3)(H_2O)_2$	2.063	2.283	157	270[d]	2710[d]
				682[e]	85.6[e]
				1092[e]	30.3[e]

[a] EPR spectra were recorded at 77 K on 0.5 mM solutions, and the field values were corrected with a gaussmeter calibrated against DPPH. Spectra of the dihalo species were obtained in dry DMSO while spectra of the diaquo species were obtained in a 50/50 EtOH/H_2O mixture. [b] Optical spectra were recorded in H_2O at 0.3−0.4 mM in the UV region and 3.0−4.0 mM in the visible region. [c] The values reported for this complex are literature values;[42] our results are essentially identical. [d] Absorptions due to LMCTs. [e] Absorptions due to d−d transitions.

Furthermore, poor donors result in copper(II) centers with increased Lewis acidity, which in turn lowers the energy of the metal d-orbitals relative to the occupied ligand orbitals, thereby decreasing the energy of the LMCT band.[38]

The frozen solution EPR spectra of $Cu([9-11]aneN_3)^{2+}$ exhibit very similar spectroscopic parameters, with $g_\parallel > g_\perp$ and large $A_\parallel$ values (Table 3). These are features characteristic of a $d_{x^2-y^2}$ ground state (i.e., a square pyramidal ground state)[35,36,39] and provide further evidence for all three complexes possessing similar geometries in solution. Interestingly, when EPR spectra of the various metal complexes were being collected, it was observed that the samples prepared in DMSO gave different values for $A_\parallel$ and $g_\parallel$ than the samples prepared in 50/50 EtOH/H_2O. Furthermore, the addition of small amounts of water to the DMSO samples yielded spectra with two sets of $g_\parallel$ signals. One set corresponded to the signals observed in dry DMSO while the second set corresponded to those seen in EtOH/H_2O. As expected, when excess H_2O was added to the DMSO samples, only the second set of peaks was observed. Therefore, it appears likely that one signal is due to a dihalo copper species and the other to an aquated copper species. In dry DMSO, the dihalo species is observed, while in 50/50 EtOH/H_2O, or after addition of excess water to the DMSO samples, only aquated species are observed. A summary of the EPR and UV/vis results is listed in Table 3.

Kinetics. Numerous experiments have demonstrated the importance of a metal-bound hydroxide in phosphodiester hydrolysis.[10,12,16,18,40] In order to compute the rates of phosphodiester hydrolysis by the different metal complexes in an unbiased manner, it was therefore necessary to perform the reactions at a pH where most of the monomeric species contained one coordinated water and one coordinated hydroxide, i.e., the catalytically active species. At this pH the effect of the equilibrium constant K_1 (Scheme 3) on the rate of hydrolysis is negligible. The pH titration curves reveal that the pK_a is strongly influenced by the size of the macrocyclic ligand; the pK_a increases as the size of the ring increases from a nine-membered ring to an 11-membered ring (Table 4). It should be noted, however, that because the monomer−dimer equilibrium depicted in Scheme 2 is pH-dependent,[5] the observed pK_a is not exactly the pK_a of the coordinated water. Instead, the observed pK_a is a composite of multiple pH-dependent equilibria. Nonetheless, the pK_a determined by titration coincides with the kinetically relevant pK_a as determined by the pH versus rate profile.[16] The results from the titration experiments indicate that, at a pH of approximately 9.2, over 90% of the monomeric species will be catalytically active for all three metal complexes. Kinetic experiments were therefore performed at this pH.

Table 4. Summary of pK_a Values, Dimer Formation Constants, and Rate Constants for the Hydrolysis of the Activated Phosphodiester BNPP by Various Metal Complexes

	pK_{a1}[a]	K_f (M^{-1})[c]	k ($M^{-1/2}$ s^{-1})[c]
$Cu([9]aneN_3)^{2+}$	7.3[b]	13000	2.0×10^{-4}
$Cu([10]aneN_3)^{2+}$	7.6	5300	4.0×10^{-4}
$Cu([11]aneN_3)^{2+}$	8.2	2700	16×10^{-4}

[a] This apparent pK_a is *not* the pK_a of the coordinated water, but rather a composite of multiple pH-dependent equilibria.[5] [b] Data taken from Deal and Burstyn.[16] [c] Reactions were performed at pH 9.2 (buffered with 50 mM CHES) and 50 °C with an ionic strength of 0.1 M (adjusted with $NaClO_4$). Becuase K_f is pH-dependent (Scheme 2),[5,16] the reported K_f values are valid at pH 9.2 only.

Interestingly, insofar as the metal−ligand formation constant is a measure of the donor strength of the triamine ligand, the observed pK_a's seem contradictory to the reported formation constants. Typically a decrease in the ligand donor strength correlates with a decrease in the pK_a of coordinated water, an indicator of increased Lewis acidity. Zompa determined[37] that as the size of the macrocycle increased from a nine- to an 11-membered ring, the formation constant decreased by over an order of magnitude, from $10^{15.5}$ to $10^{14.4}$. Therefore, the 11-membered ring is presumably a poorer electron donor than the nine-membered ring and, as a result, $Cu([11]aneN_3)^{2+}$ should be a stronger Lewis acid than $Cu([9]aneN_3)^{2+}$. This conclusion is supported by the energies of the ligand field transitions; as the size of the macrocycle increases, the d−d absorption shifts to longer wavelengths (Table 3) consistent with a decrease in the d−d splitting, Δ. The observed increase in the pK_a as the size of the macrocycle increases is a consequence of the multiple pH-dependent equilibria. Both the monomer−dimer equilibrium and the deprotonation of the coordinated water contribute to the measured pK_a.[5]

In order to compare the reactivities of $Cu([9-11]aneN_3)X_2$ in catalyzing phosphodiester hydrolysis, a series of reactions were performed in which the catalyst and BNPP concentrations were alternately varied. Analysis using the method of initial rates revealed that the hydrolysis of BNPP follows a first-order dependence on substrate concentration and a half-order dependence on the concentration of copper complex (Figure 2). These results, which are consistent with those obtained for the hydrolysis of BNPP by $Cu([9]aneN_3)Cl_2$ at pH 7.2,[16] indicate that the metal complexes exist in a monomer−dimer equilibrium with the monomer being the active species. The rate law being known, it was then possible to calculate true 1.5-order rate constants for the hydrolysis of BNPP via regression of the plots of both [BNPP] and $[Cu]^{0.5}$ versus initial rate (Table 4). The rate constant increases by approximately an order of magnitude as the size of the ligand is increased from a nine-membered to an 11-membered ring.

It being anticipated that the dimer formation constant (K_f) would vary with ring size, K_f's were calculated from a plot of

(38) Cox, D. D.; Benkovic, S. J.; Bloom, L. M.; Bradley, F. C.; Nelson, M. J.; Que, L., Jr.; Wallick, D. E. *J. Am. Chem. Soc.* **1988**, *110*, 2026−2032.
(39) Bencini, A.; Bertini, I.; Gatteschi, D.; Scozzafava, A. *Inorg. Chem.* **1978**, *17*, 3194−3197.
(40) Koike, T.; Kimura, E. *J. Am. Chem. Soc.* **1991**, *113*, 8935−8941.

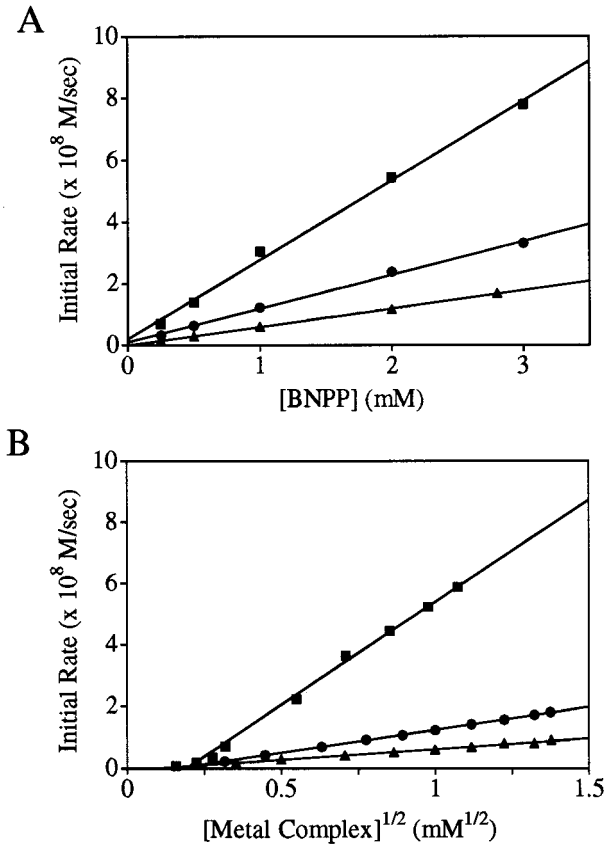

Figure 2. Determination of the rate law for the hydrolysis of BNPP by Cu([9−11]aneN$_3$)X$_2$. Reactions were carried out at pH 9.2 and 50 °C, as described in the text, with Cu([9]aneN$_3$)Cl$_2$ (△), Cu([10]aneN$_3$)Br$_2$ (●), or Cu([11]aneN$_3$)Br$_2$ (■). (A) Effect of varied [BNPP] at fixed [Cu([9−11]aneN$_3$)X$_2$] (1.0 mM). (B) Effect of varied [Cu([9−11]aneN$_3$)X$_2$] at fixed [BNPP] (1.0 mM). The derived rate law is rate = k[BNPP][Cu([9−11]aneN$_3$)X$_2$]$^{1/2}$.

initial rate versus [Cu]$^{0.5}$.[16,41] Note that, because K_f is pH-dependent (Scheme 2),[5,16] the values reported are for pH 9.2 only. The results demonstrate that as the size of the ring increases, K_f decreases substantially. As expected, there is a strong correlation between K_f and the rate constant, k, indicating that the monomer−dimer equilibrium is an important determinant in the rate of BNPP hydrolysis (Table 4); the rate increases as K_f decreases, i.e., the higher the monomer concentration, the faster the hydrolysis reaction. Using K_f to determine the relative free monomer concentrations, however, revealed that this change in the dimer formation constant cannot completely account for the increase in the rate of hydrolysis and that other factors must also be important.

To better understand the other factors affecting the rate of phosphodiester hydrolysis, reactions were performed under saturating substrate conditions. The limited solubility of BNPP in water and the low affinity of BNPP for the metal complexes made it necessary to use the more water soluble phosphodiester, ENPP, to achieve saturation. The constants K_2 and k_3 were extracted from a nonlinear least squares fit of the curve obtained from a plot of substrate concentration versus initial rate (data provided in Supporting Information). Binding of the substrate to the metal complex, however, perturbs the monomer−dimer equilibrium toward the monomer, resulting in a linearization of the saturation curve. Consequently, the values obtained for

Table 5. Summary of Kinetically Determined Rate and Equilibrium Constants for Various Metal Complexes in the Hydrolysis of the Activated Phosphodiester ENPP[a]

	K_2 or $1/K_m$ (M^{-1})	k_3 or k_{cat} (s^{-1})
Cu([9]aneN$_3$)(OH)(H$_2$O)$^+$	3 ± 1	$5 \pm 2 \times 10^{-4}$
Cu([10]aneN$_3$)(OH)(H$_2$O)$^+$	2.7 ± 0.7	$4 \pm 1 \times 10^{-4}$
Cu([11]aneN$_3$)(OH)(H$_2$O)$^+$	5.0 ± 0.7	$3.4 \pm 0.4 \times 10^{-4}$

[a] Reactions were performed at pH 9.2 (buffered with 0.5 M CHES) and 50 °C with an ionic strength of 0.68 M (adjusted with 0.5 M NaClO$_4$). The rate constant k_3 was calculated by dividing V_{max} by the total catalyst concentration. Values for K_2 and k_3 were corrected to take into account the monomer−dimer equilibrium of the metal complexes using the method outlined in the Experimental Section.

K_2 and k_3 ($1/K_m$ and k_{cat} using enzymatic nomenclature) were too low and too high, respectively. The results obtained from the nonlinear least squares fit were therefore corrected using the method outlined in the Experimental Section. These corrected values (Table 5) indicate that as the size of the ring increases, the affinity of the metal complex for ENPP (K_2) also increases while k_3 remains constant within experimental error. The large uncertainties in K_2 and k_3 are a result of the difficulty in saturating the metal complexes with substrate due to the metal complexes' low affinity for ENPP and the perturbation in the monomer−dimer equilibrium upon substrate binding.

True 1.5-order rate constants were calculated for the hydrolysis of ENPP and found to be approximately 2 orders of magnitude smaller than the rate constants for the corresponding reactions with BNPP. This decrease can be explained by the fact that ENPP contains only a single 4-nitrophenyl group while BNPP contains two 4-nitrophenyl groups. Because the reaction occurs via a concerted mechanism,[17] the nucleophile must attack trans to the leaving group; this is 50% less likely with ENPP as with BNPP, and therefore BNPP is intrinsically more reactive. It was also necessary to perform the ENPP saturation kinetics under conditions of much higher buffer concentration and ionic strength, both of which are known to cause a decrease in the rate of hydrolysis of phosphodiesters by Cu([9]aneN$_3$)Cl$_2$.[16] Thus, the smaller rate constants observed with ENPP relative to BNPP were to be expected.

Discussion

Structural Analysis. The crystal structures for Cu([9]aneN$_3$)Cl$_2$, Cu([10]aneN$_3$)Br$_2$, and Cu([11]aneN$_3$)Br$_2$ (Figure 1) show an interesting structural trend, changing from a square pyramid for Cu([9]aneN$_3$)Cl$_2$ toward a distorted trigonal bipyramid for Cu([11]aneN$_3$)Br$_2$. (It should be noted that the published crystal structures of Cu([9]aneN$_3$)Cl$_2$[27] and Cu([9]aneN$_3$)Br$_2$[42] are very similar, indicating that the differences in geometry between the three different complexes described herein cannot be attributed to the coordinated halide ions.) The unit cell of Cu([10]aneN$_3$)Br$_2$ contains two crystallographically independent molecules with one structure best described as a square pyramid and the other best described as a distorted trigonal bipyramid. Despite the obvious similarities between the three complexes, there are two distinctive features which warrant the different descriptions of their respective geometries. The first key feature is their τ-value. As discussed previously, a τ-value of 0.00 is considered to be indicative of a perfect square pyramidal structure while a τ-value of 1.00 denotes a trigonal bipyramid.[35] According to this criterion, Cu([9]aneN$_3$)Cl$_2$ ($\tau = 0.02$) and Cu([10]aneN$_3$)Br$_2$ [10a] ($\tau = 0.00$) clearly have a different geometry from

(41) The rate equation from which the K_f analysis is derived assumes that loss of the product is rate limiting, i.e., $k_3 \ll k_{-2}$ in Scheme 3.[16]

(42) Bereman, R. D.; Churchill, M. R.; Schaber, P. M.; Winkler, M. E. *Inorg. Chem.* **1979**, *18*, 3122−3125.

Cu([10]aneN$_3$)Br$_2$ [10b] (τ = 0.61) and Cu([11]aneN$_3$)Br$_2$ (τ = 0.58). The second important feature is the difference in the axial and equatorial Cu−N bond lengths. Whereas the axial Cu−N bond is longer than the two equatorial Cu−N bonds in the square pyramidal geometry, the axial Cu−N bond is shorter in the trigonal bipyramidal geometry. Shortening of the axial Cu−N bond relative to the equatorial Cu−N bonds was observed previously in other trigonal bipyramidal structures and attributed to greater σ-donation by the axial nitrogen atoms.[43]

It is useful to correlate the structures of the three Cu(II) complexes with the constraints imposed by the macrocyclic tridentate ligand. Ligand field stabilization energy provides very little preference for either the square pyramidal or trigonal bipyramidal geometries in a d^9 metal complex; the two geometries are very similar in energy.[44] Thus, the different geometries observed in the crystal structures of Cu([9−11]aneN$_3$)X$_2$ may simply reflect different crystal packing forces. This possibility is supported by the observation that the solution spectroscopic characteristics are consistent with a square pyramidal structure for all three complexes. In the structure of Cu([9]aneN$_3$)Cl$_2$, the ethylene bridges between the nitrogen atoms constrain all three N−Cu−N angles to approximately 82.5(2)°. It is not surprising, therefore, that the complex adopts a square pyramidal structure where the idealized N−Cu−N angles are all 90° as opposed to a trigonal bipyramidal structure where one of the idealized N−Cu−N angles is 120°. In the case of Cu([11]aneN$_3$)Br$_2$, however, two of the N−Cu−N angles have increased to approximately 100°, and the complex crystallizes in a distorted trigonal bipyramidal geometry. Yet if the constraints of the ligand were important in determining the geometry of the complex, one would expect that the N−Cu−N equatorial angle would be the largest N−Cu−N angle in the two trigonal bipyramidal structures (in an idealized structure N$_{eq}$−Cu−N$_{eq}$ is 120° while the two N$_{eq}$−Cu−N$_{ax}$ angles are 90°). As shown in Table 2, however, this is not the case. In fact, the single propylene bridge does not span the equatorial nitrogen atoms in Cu([10]aneN$_3$)Br$_2$, and the angle is still considerably strained at 84.7(3)°. A consistent feature in the two independent structures of Cu([10]aneN$_3$)Br$_2$, regardless of the best geometrical description of the complex, is the sum of the three N−Cu−N angles. The total angle subtended by the ligand remains constant at 257° and provides a measure of the steric demand of the ligand within the coordination sphere of the Cu(II) ion. Moreover, for each ligand the volume occupied by the macrocycle is likely to be independent of the specific geometry. Therefore, the solid state structure provides a reasonable measure of the steric bulk of the ligand even though the geometry in solution may be different from that determined in the solid state.

Kinetics. A proposed mechanism for the hydrolysis of activated phosphodiesters by Cu([9]aneN$_3$)Cl$_2$ has been previously described in detail (Schemes 2 and 3).[16,17] Given the similarities between the complexes, one would predict that Cu([10]aneN$_3$)Br$_2$ and Cu([11]aneN$_3$)Br$_2$ would catalyze the hydrolysis of phosphodiesters via the same mechanism as Cu([9]aneN$_3$)Cl$_2$. To test the validity of this assumption, we determined the rate law for the hydrolysis of BNPP by each of the three complexes. All reactions exhibit a first-order dependence with respect to substrate concentration and a half-order dependence on metal concentration; the half-order dependence on catalyst concentration indicates the presence of a monomer−dimer equilibrium with the monomer being the catalytically active species. The fact that all three complexes obey the same rate law when hydrolyzing BNPP is evidence for identical mechanisms, and we have therefore assumed that Schemes 2 and 3 can be generalized to Cu([9−11]aneN$_3$)X$_2$.

One of the salient features of the mechanism of BNPP hydrolysis by Cu([9−11]aneN$_3$)X$_2$ is the presence of a monomer−dimer equilibrium in the metal complex. This equilibrium is a key control element in the overall rate of the reaction since a lower formation constant, K_f, results in a higher concentration of active monomeric catalyst.[16] The crystallographic data for the three complexes reveals that as the ligand ring increases in size and becomes more flexible, the copper atom lies closer to the plane of the three nitrogen atoms, presumably causing a destabilization of the dimer due to steric effects. (The importance of steric constraints in determining the magnitude of K_f is even more obvious when one considers that, solely on the basis of electronic arguments, Cu([11]aneN$_3$)Br$_2$ should have the largest formation constant since it is the strongest Lewis acid.) A simple calculation using K_f to determine the relative monomer concentrations,[16] however, reveals that the difference in K_f is not enough to account for a rate constant increase of nearly an order of magnitude. Therefore, additional factors must also influence the rate of hydrolysis.

On the basis of results obtained using various Co(III) complexes, it has been suggested that as the bond angle between the two labile cis-oriented sites decreases, the rate of hydrolysis increases.[13] The rationale is that the four-membered-ring transition state formed from the intramolecular attack of the metal-bound hydroxide on the coordinated substrate is stabilized by a smaller O−M−O angle.[13] The crystal structures of Cu([9−11]aneN$_3$)X$_2$ reveal that there is a decrease in the angle from 94.23(5)° to 90.50(5)° between the two labile cis-oriented sites as the ligand size increases and the metal sits closer to the plane defined by the three nitrogen atoms. It is tempting to use this compression of the cis bond angle as another contributing factor to account for the increase in the rate of hydrolysis as the ligand increases in size from [9]aneN$_3$ to [10]aneN$_3$ to [11]aneN$_3$. If the compression of the cis angle were a significant factor in this case, however, then one would expect to see a corresponding increase in k_3, the rate of intramolecular attack on the coordinated substrate. The k_3 values obtained for the hydrolysis of ENPP, however, are identical within experimental error (Table 5). The difference between the cobalt(III) complexes[13] and the copper(II) complexes described herein may be attributed to the fact that the O−Co−O core is considerably stiffer than the corresponding O−Cu−O core.[45,46] Thus, because the copper complexes are easier to deform, the resting O−Cu−O angle does not significantly influence the rate of catalysis.

A second factor likely to affect k_3 is the Lewis acidity of the metal complex. In the Cu([9−11]aneN$_3$)X$_2$ series, the Lewis acidity increases with the size of the macrocycle due to the poorer donor ability of the larger rings.[37] This trend of increasing Lewis acidity with increasing macrocycle size can be observed in the UV/vis spectra (Table 3), where the poorer donor ability of the larger rings results in a shift of both the d−d band and the LMCT band to lower energy as the Lewis acidity increases.[38] (As discussed in the Results section, the measured pK_a is not an accurate gauge of the Lewis acidity since this apparent pK_a is a composite of multiple pH-dependent equilibria.[5]) Since Cu-

(43) Gerloch, M.; Deeth, R. J. *Inorg. Chem.* **1984**, *23*, 3853−3861.
(44) Cotton, F. A.; Wilkinson, G. *Advanced Inorganic Chemistry*, 5th ed.; John Wiley & Sons: New York, 1988.
(45) Comba, P.; Hambley, T. W. *Molecular Modeling of Inorganic Compounds*; VCH Publishers: Weinheim, 1995.
(46) Comba, P.; Hambley, T. W.; Strohle, M. *Helv. Chim. Acta* **1995**, *78*, 2042−2047.

([11]aneN$_3$)Br$_2$ is a stronger Lewis acid than Cu([9]aneN$_3$)Cl$_2$ and Cu([10]aneN$_3$)Br$_2$, Cu([11]aneN$_3$)Br$_2$ is expected to activate the coordinated phosphodiester toward nucleophilic attack to a greater degree than the other complexes. Thus, once again we would expect k_3 to be larger for Cu([11]aneN$_3$)Br$_2$ relative to Cu([9]aneN$_3$)Cl$_2$ and Cu([10]aneN$_3$)Br$_2$. According to Table 5, however, this is not the case. One explanation for the apparent lack of correlation between the Lewis acidity and k_3 is that as the metal complex becomes a stronger Lewis acid, the nucleophilicity of the coordinated hydroxide decreases, which is expected to decrease k_3. Because the effects of increased substrate activation and decreased nucleophilicity of the coordinated hydroxide counter one another, the effect of Lewis acidity on k_3 cannot be determined with any degree of certainty.

The equilibrium constant for the formation of the catalyst−substrate complex, K_2, is also expected to greatly affect the rate of hydrolysis. Results from the reactions performed under saturating ENPP conditions indicate that while the K_2's are equal within experimental error for Cu([9]aneN$_3$)Cl$_2$ and Cu([10]aneN$_3$)Br$_2$, Cu([11]aneN$_3$)Br$_2$ has a slightly larger K_2 (Table 5). This result initially seems counterintuitive since one anticipates that K_2 will decrease with increasing ligand size due to steric effects as the metal is pulled into the plane of the ligand. However, K_2 is also expected to increase with increasing Lewis acidity. Since the 11-membered-ring is a poorer donor to the copper(II) center,[37] Cu([11]aneN$_3$)$^{2+}$ is a stronger Lewis acid relative to Cu([9]aneN$_3$)$^{2+}$ and Cu([10]aneN$_3$)$^{2+}$ and, therefore, should have a larger K_2. Thus, Lewis acidity is more important than steric constraints in determining the magnitude of the catalyst−substrate formation constant.

Conclusion

The results obtained by Chin et al. on the reactivity of a series of tetraamine−Co(III) complexes suggested that a major factor affecting the differences in rate of phosphodiester hydrolysis in those systems is the N−Co−N angle and the corresponding ability of the complexes to stabilize the four-membered-ring transition state. The results described herein, however, indicate that for Cu(II) macrocycles, the situation is far more complex. The ability to stabilize the four-membered-ring transition state is not an important consideration in these systems on the basis of the fact that k_3 is identical within experimental error for Cu([9−11]aneN$_3$)X$_2$. This can be rationalized by the fact that the O−M−O core is significantly easier to deform in Cu(II) complexes than in corresponding Co(III) complexes. The monomer−dimer equilibrium, however, does play a key role in the rate of phosphodiester hydrolysis, although this factor alone cannot account for the differences in reactivity in the Cu([9−11]aneN$_3$)X$_2$ series. Other factors such as Lewis acidity, the geometry, and the conformational flexibility of the complexes may also be important and will be the subject of future studies.

Acknowledgment. The authors thank Dr. Marcel Hop (University of Wisconsin−Madison) for obtaining mass spectral data. The authors also gratefully acknowledge Professors A. C. Hengge (Utah State University) and W. W. Cleland (University of Wisconsin−Madison) for their helpful discussions and expertise in saturation kinetics and Professor W. B. Tolman (Univeristy of Minnesota) for timely discussions on spectroscopy. Funding was provided by the Alfred P. Sloan Foundation (J.N.B.), the NIH Biotechnology Training Grant (E.L.H.), the Wisconsin/Hilldale Undergraduate/Faculty Research Award (S.H.M.), and the University of Wisconsin Graduate School Research Committee.

Supporting Information Available: Saturation kinetics data as well as the Fortran program, equations, and procedure used to determine the correction factor for K_m and V_{max}. An X-ray crystallographic file, in CIF format, for Cu([10−11]aneN$_3$)Br$_2$. This material is available free of charge via the Internet at http://pubs.acs.org.

IC981087G